



**HAL**  
open science

## Bayesian filter for failure times identification of moving heat sources in 2D geometry

Mohamed Salim Bidou, Sylvain Verron, Laetitia Perez, Laurent Autrique

► **To cite this version:**

Mohamed Salim Bidou, Sylvain Verron, Laetitia Perez, Laurent Autrique. Bayesian filter for failure times identification of moving heat sources in 2D geometry. *International Journal of Systems Science*, 2024, 55 (4), pp.671-686. 10.1080/00207721.2023.2293682 . hal-04470260

**HAL Id: hal-04470260**

**<https://univ-angers.hal.science/hal-04470260>**

Submitted on 21 Feb 2024

**HAL** is a multi-disciplinary open access archive for the deposit and dissemination of scientific research documents, whether they are published or not. The documents may come from teaching and research institutions in France or abroad, or from public or private research centers.

L'archive ouverte pluridisciplinaire **HAL**, est destinée au dépôt et à la diffusion de documents scientifiques de niveau recherche, publiés ou non, émanant des établissements d'enseignement et de recherche français ou étrangers, des laboratoires publics ou privés.

RESEARCH ARTICLE

## Bayesian filter for failure times identification of moving heat sources in 2D geometry

Mohamed Salim Bidou<sup>a</sup>, Sylvain Verron<sup>a</sup>, Laetitia Perez<sup>a</sup>, Laurent Autrique<sup>a</sup>

<sup>a</sup>LARIS, Polytech, University of Angers, 62 avenue notre dame du lac, 49000 Angers, France.

### ABSTRACT

This study investigates the application of the Bayesian filter method for identifying failure times in a 2D parabolic partial differential equation system. The identification of failure times in thermal systems, which are subject to partial differential equations, presents significant difficulties, especially due to their ill-posed nature, which makes them highly sensitive to measurement errors. A Bayesian inference framework was previously developed in a related study, aiming to solve inverse heat conduction problems by utilizing temperature measurements from sensors to estimate failure times or potential restarts of fixed heat sources. This paper focuses on the case of mobile sources, where a set of fixed sensors is considered and the trajectories of the heating sources are known and follow a constant velocity. The main objective is to accurately identify the failing heat sources and determine the exact failure time, as well as the possibility of resuming normal operation. A Monte Carlo simulation is performed to assess the impact of sensor measurements.

### KEYWORDS

Failure times identification; fault diagnosis; kalman filters; heat measurement; inverse problems; partial differential equations

## 1. Introduction

Due to the growing complexity of industrial systems and the growing concern for their safety, there has been an increase in interest in fault diagnosis in recent decades. The use of theories based on partial differential equations (PDEs) has become prevalent in

## Nomenclature

$\Delta t$	time step, s	$e$	thickness, m
$\Delta t_{obs}$	time step of the observations, s	$h$	natural convection coefficient
$\Delta x, \Delta y$	space step, m		Natural convection coefficient,
$\Gamma$	boundary of $\Omega$		$W \cdot m^{-2} \cdot K^{-1}$
$\lambda$	thermal conductivity, $W \cdot m^{-1} \cdot K^{-1}$	$T$	temperature, K
$\Omega$	geometric domain	$t$	time, s
$\vec{n}$	unit external outward-pointing vector	$t_f$	final time, s
$\rho C$	volumetric heat, $J \cdot m^{-3} \cdot K^{-1}$	$T_0$	initial temperature, K
		$x$	space variable, m
		$y$	space variable, m

modeling various phenomena within complex physical systems. For instance, Fourier's law in thermal sciences, which governs heat exchange, leads to a system of parabolic PDEs. Ordinary differential equations (ODEs) are insufficient for accurately capturing the dynamic behaviors of most practical engineering models due to their limited ability to account for spatial and temporal evolution. Model-based fault detection and diagnosis systems have emerged as a prominent approach for addressing these challenges. Faults are characterized as malfunctions in system components, sensors, or actuators. If these faults go undetected and unaddressed during system operation, they can severely impact the overall system performance, leading to system failure or significant human and material losses. Thus, timely and accurate fault detection plays a crucial role in ensuring system reliability and preventing adverse consequences.

In industrial heating systems, failures in heating sources can lead to decreased efficiency, product quality issues, or safety hazards. Heating, ventilation, and air conditioning (HVAC) systems require accurate identification of failure times to ensure temperature consistency, energy efficiency, and occupant comfort. Power generation plants heavily rely on heating sources, and any faults can result in power outages or reduced capacity. Solar thermal systems, which utilize sunlight as a heating source, require reliable fault detection to maximize energy output. Process industries, such as petrochemical plants or food processing facilities, depend on thermal systems, and timely fault detection is crucial for maintaining production schedules, ensuring product quality, and preventing safety risks.

The field of controlling and estimating of PDEs has been an active area of research for several decades. There are generally two approaches for PDE control and estimation: (i) Early lumping, where the PDEs is approximated by ODEs and the design is conducted in a finite-dimensional space (Cheng et al., 2009; Wu & Li, 2008); and (ii) Late lumping, which involves designing in an infinite-dimensional space and directly studying the PDEs without using approximate methods (Krstic & Smyshlyaev, 2008; Wu et al., 2011). While control and estimation research has received significant attention, system fault diagnosis, on the other hand, has been relatively less explored. Existing PDEs diagnostic schemes mainly employ early lumping approaches (Demetriou, 2002; El-Farra & Ghan-tasala, 2007; Ghantasala & El-Farra, 2009; Ju et al., 2021; Pourdadashi Komachali & Shafiee, 2020). The early lumping method has been extensively employed in early research on system fault diagnosis utilizing PDEs modeling. Nevertheless, this approach suffers from certain drawbacks. The finite dimensional approximation frequently results in the loss of crucial intrinsic characteristics inherent in the original PDEs model. The other “late lumping” based on PDEs observer-based fault diagnosis schemes has been successfully applied to parabolic systems in research projects such as (Cai et al., 2016; Duan & Patton, 2001; Feng et al., 2022; Ferdowski et al., 2022, 2023; Frank, 1994; Lei et al., 2022).

This article presents an approach for identifying failure times in heating sources within a thermal system using a parametric estimation method. Within the framework of parametric estimation, it is reasonable to view the search for failures in a system governed by a PDE system under normal conditions as an inverse problem (Bidou et al., 2022b). Consequently, in the thermal domain, a Bayesian-based approach is employed to solve Inverse Heat Conduction Problems (IHCPs).

In recent years, there has been significant development in Bayesian approaches for solving IHCPs (Patel et al., 2022; Yeonjong et al., 2020; Yin et al., 2021). These approaches utilize statistical inference to estimate unknown parameters based on their probability density functions, which are defined using observed data. State estimation problems have also been addressed using Bayesian filter-based approaches. The Kalman filter (KF) (Kalman, 1960) is a widely used Bayesian filter, but its applicability is limited to linear models with additive Gaussian noise. Currently, there is active

research on applying the KF to inverse heat transfer problems. The Kalman procedures in the time domain, including filtering, smoothing, and prediction, have been utilized in various studies. For instance, in Massard et al. (2012), a KF-based method was developed to estimate the intensity and positioning of a heating flux on a plate at each instant, allowing for the estimation of a source's trajectory. Similarly, in Wang et al. (2020), a real-time method based on KF was proposed and improved to locate a moving heat source in a three-dimensional heat transfer system. In Gaaloul & Daouas (2018), the Kalman smoother (KS) was employed to inversely estimate the heat flux on the front and back surfaces of a cylindrical nonlinear two-dimensional system using future temperature data from the back surface. The KS method was also utilized in Wen et al. (2020) to resolve the inverse estimation of radiation-conduction problems by combining the KF and Rauch-Tung-Striebel smoothing (Rauch et al., 1965).

In the context of parametric estimation, the identification of failure times in a system governed by a set of PDEs, representing its fault-free behavior, can be viewed as an inverse problem. Consequently, failure instants within the thermal framework can be identified by solving an IHCPs based on observations obtained from the malfunctioning system. However, there are several important considerations to address. Firstly, IHCPs are highly sensitive to measurement errors due to their ill-posed nature (Alifanov, 1994). Additionally, the failures under investigation are characterized as "on-off" events, and the study's structure bears resemblance to hybrid systems with delays caused by discontinuous switching associated with heat transport phenomena.

To tackle these challenges, a methodology was proposed in our previous work (Bidou et al., 2022a) for estimating failures and restarts of heat sources. This approach is based on the KS and uses a search strategy by solving an optimization problem. It is important to note that the previous work primarily focused on fixed heat sources. However, in order to address a more challenging scenario, we further explore the case of mobile heat sources with known trajectories. Unlike fixed sources, mobile heat sources introduce additional complexities in accurately identifying which specific heat source has failed and determining the exact time of failure. The mobility of heat sources adds dynamism to the system as the sources continuously move along their known trajectories.

The structure of this article is organized as follows. Section 2 provides a detailed description of the physical problem formulation in a two-dimensional geometry. In Section 3, we introduce a Bayesian filter based on conventional Kalman filtering and smoother techniques to address the inverse problem. This section begins by formulating the direct problem as a state estimation problem, followed by the presentation of the inverse problem. We then propose a methodology for estimating failure and restart instants using a search strategy that considers various candidate signals from the heating sources. Section 4 presents and discusses the numerical results obtained for both fixed and mobile heat sources. Finally, the study concludes in Section 5, where we provide an overview of the main findings and outline potential directions for future research.

## 2. Application description

### 2.1. The direct problem

The application given here is a 1 meter long by 1 meter wide by 2 mm thick aluminum plate. On this are positioned four temperature sensors and three heating sources. The locations of the three sources and four sensors are known. The behavior of the heating sources is unpredictable. These, specifically, will encounter all-or-nothing failures. Consequently, a source may stop operating (in which case its heat flow would be zero) and then return to its regular behavior, and this could occur frequently.

Let's define the geometric domain as  $\Omega = [-0.5, 0.5]^2 \subset \mathfrak{R}^2$  and every point in space possesses coordinates  $(x, y) \in \Omega$ . The time variable is  $t \in [0, t_f]$ .  $T(x, y, t)$  represents the temperature at every point in space. The following set of mathematical equations (Vergnaud et al., 2016) describes the temperature's temporal evolution in the  $\Omega$  domain:

$$\left\{ \begin{array}{l} \rho C \frac{\partial T(x, y, t)}{\partial t} - \lambda \Delta T(x, y, t) = \frac{q(x, y, t) - 2h(T(x, y, t) - T_0)}{e}, \quad (x, y, t) \in \Omega \times [0, t_f], \\ T(x, y, 0) = T_0, \quad (x, y) \in \Omega, \\ -\lambda \frac{\partial T(x, y, t)}{\partial \vec{n}} = 0, \quad (x, y, t) \in \Gamma \times [0, t_f], \end{array} \right. \quad (1)$$

where  $\Delta$  is the Laplacian operator:

$$\Delta T(x, y, t) = \frac{\partial^2 T(x, y, t)}{\partial x^2} + \frac{\partial^2 T(x, y, t)}{\partial y^2}.$$

It is crucial to mention that the previous mathematical model is based on knowledge of physical behavior perfectly described by physical law. Such a white box model in thermal sciences is issued from Fourier's law leading to direct problem (1). In general, this so called heat equation (parabolic PDE) is considered in order to describe energy balance and is adapted to conductive, convective and radiative exchanges (see for example H.S. Carslaw & Jaeger, 1986). For both convective and radiative transfers grey boxes models could be additionally taken into account. Thus, in the following a valid mathematical model is implemented in order to develop a whole methodology adapted to a wide range of experimental configurations. Examples can be proposed in L. Autrique et al., 2009 ; Lascoup et al., 2014 ; Museux et al., 2012. Thermophysical parameters of the considered metallic plate are issued from Ashby, 1993. The input parameters for the model are listed in Table 1. Figure 1 illustrates the locations of the sources and sensors.

Table 1.: Mathematical model input parameters.

Symbol	Definition	Values
$\rho C$	Volumetric heat	$2.421 \cdot 10^6 \text{ J} \cdot \text{m}^{-3} \cdot \text{K}^{-1}$
$h$	Natural convection coefficient	$10 \text{ W} \cdot \text{m}^{-2} \cdot \text{K}^{-1}$
$\lambda$	Thermal conductivity	$178 \text{ W} \cdot \text{m}^{-1} \cdot \text{K}^{-1}$
$T_0$	Initial temperature	293 K
$t_f$	Final time	3600 s
$e$	Thickness	$2 \cdot 10^{-3} \text{ m}$

Several heating sources contribute to the heat flux  $q(x, y, t)$ :

$$q(x, y, t) = \sum_{i=1}^{n_{\text{heat}}} q_i(x, y, t), \quad \text{with: } n_{\text{heat}} = 3. \quad (2)$$

Each heat source,  $q_i(x, y, t)$ , can be described by the product of three separate func-

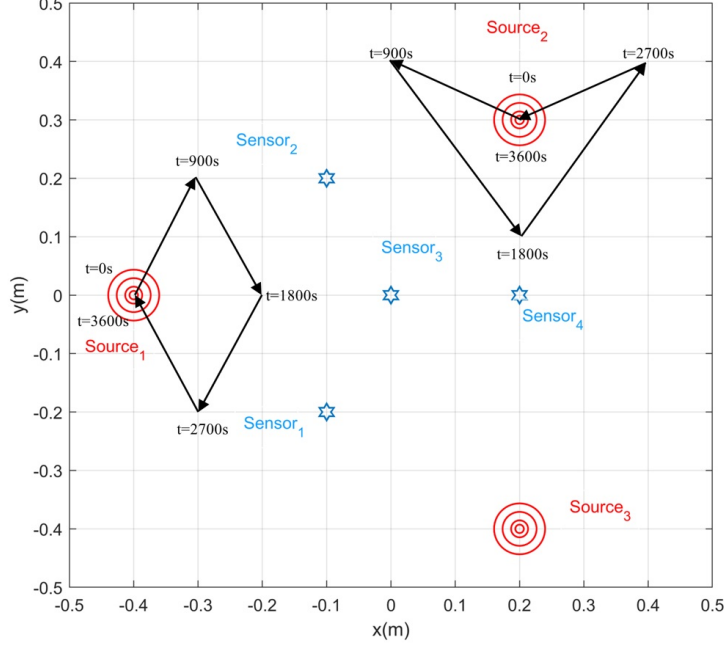


Figure 1.: Positions of the plate's 3 sources and 4 sensors.

tions:

$$q_i(x, y, t) = \psi_i(x, y, t)\phi_i(t)g_i(t), \quad (3)$$

the function  $\psi_i(x, y)$  determines the spatial support of the heat source and represents its spatial distribution. It is modeled as a Gaussian distribution centered at the point  $(x_i, y_i)$ :

$$\psi_i(x, y, t) = \exp\left(-\frac{(x - x_i(t))^2 + (y - y_i(t))^2}{(5 \times 10^{-2})^2}\right). \quad (4)$$

The spread of the Gaussian is controlled by a standard deviation of  $5 \times 10^{-2}$ . This function essentially quantifies the extent to which each source influences its surrounding region. The function  $\phi_i(t)$  characterizes the temporal behavior of each heat source, representing the normal heat flux generated by source  $i$ . It describes how the heat flux changes over time for each specific source. The plot in Figure 2 illustrates the evolution of the heat flux for the three sources. Moreover, the function  $\chi_i(t)$  is introduced to

account for possible faults or failures in heating source  $i$ :

$$\varrho_i(t) = \begin{cases} 1 & \text{without failure,} \\ 0 & \text{in case of failure.} \end{cases} \quad (5)$$

This function serves as an indicator, assuming a value of 1 when the source is operating without any failure and 0 in the event of a failure. The occurrence of failures is represented by discontinuous steps in the function  $\varrho_i(t)$ , transitioning between 1 and 0, or vice versa. If a heating source experiences a failure, a step from 1 to 0 is observed, indicating a cessation of heat generation. Conversely, a step from 0 to 1 signifies the successful restart of a previously failed source. An example demonstrating the behavior of the function  $\varrho_i(t)$   $i = 1, 2, 3$  is depicted in Figure 3. In this example, source 1 experiences a failure at 1000s and restarts operation at 2500s, source 2 fails at 2000s, and source 3 operates without any failure.

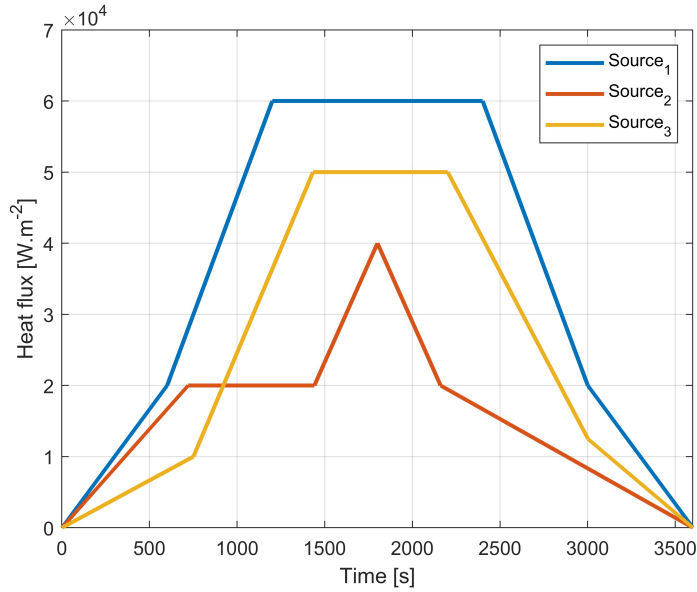


Figure 2.: The flux of the three sources  $\phi_1(t)$ ,  $\phi_2(t)$ , and  $\phi_3(t)$  in normal operation, without any failures.

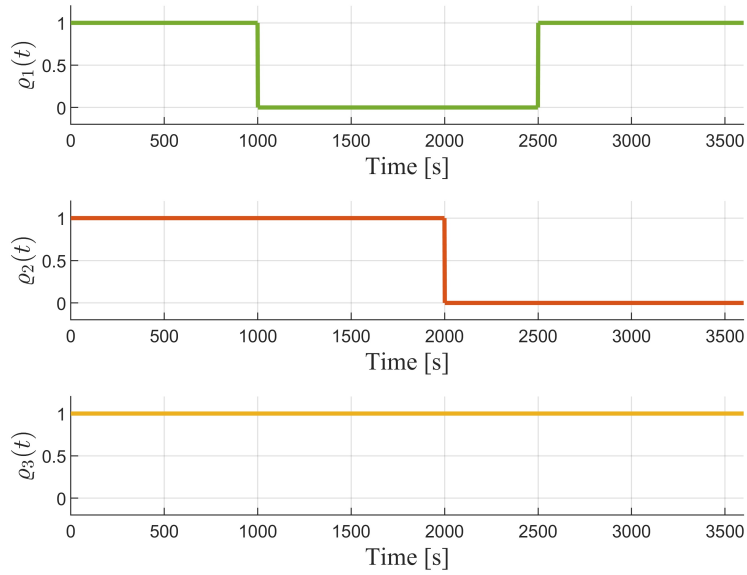


Figure 3.: Illustrations of  $\varrho_1(t)$ ,  $\varrho_2(t)$  and  $\varrho_3(t)$ .

### 3. The inverse problem

#### 3.1. State estimation problem

State estimation inverse problems are highly relevant in practical applications (J. Kaipio & Somersalo, 2006; J. P. Kaipio & Fox, 2011; Özisik & Orlande, 2021). These problems involve the estimation of dynamic variables using observable data and prior knowledge of physical processes. They are typically addressed through Bayesian filters. The KF is the most widely used Bayesian filter method, particularly for linear models with additive Gaussian noises. In order to address the evolution and observation problems within this framework, it is necessary to redefine the direct problem (1). A numerical approach utilizing the finite difference method is proposed for this task (Özisik et al., 2017). The discretization of the system (1) using finite differences and the construction of the evolution and observation models are explicitly demonstrated and analyzed in Bidou et al. (2022a). Consequently, the application can be formulated

as follows:

$$\begin{cases} \mathbf{T}^{k+1} = \mathbf{L} \cdot \mathbf{T}^k + \mathbf{B}^k \cdot \mathbf{G}^k + \mathbf{H}, \\ \mathbf{T}_{obs}^k = \mathbf{C} \cdot \mathbf{T}^k. \end{cases} \quad (6)$$

In the discretized evolution problem,  $\mathbf{T}^k$  represents the matrix of temperature values at all discretized points on the plate at the discrete time step  $k$ . The transition matrix  $\mathbf{L}$  is pivotal as it encodes the linear relationships between the states at time step  $k$  and  $k + 1$ , effectively determining the progression of the system in time due to conductive heat transfer.

The core aspect of modeling moving sources is encapsulated in the function  $q_i(x, y, t)$  and  $\psi_i(x, y, t)$  in equations (3) and (4), which defines the spatial support of the heat source, represented by a Gaussian distribution centered around a time-dependent point  $(x_i(t), y_i(t))$ . This Gaussian distribution captures the spatial influence of the heat source, with its mobility directly influencing the temperature distribution within the domain  $\Omega$ .

In transitioning to an evolution problem, this mobile characteristic is embedded within the matrix  $\mathbf{B}^k$ . For each time step  $k$ , the matrix  $\mathbf{B}^k$  is recalculated to reflect the new positions of the moving heat sources. This is crucial as the Gaussian distribution, which represents the spatial influence of each source, changes its center according to the source's trajectory  $(x_i(t), y_i(t))$ . In essence,  $\mathbf{B}^k$  dynamically updates the spatial weighting of the heat source's influence within the grid at each time step, ensuring that the model captures the mobility of the sources. In the case of fixed sources, the heat flux is consistent over time, and therefore  $\mathbf{B}^k$  reduces to a static matrix  $\mathbf{B}$ , reflecting the unchanging position of the Gaussian distribution centers  $(x_i, y_i)$ .

The heat flux for each source at each time step  $k$ , denoted in equation (3) by  $\phi_i^k$  for  $i = 1, \dots, 3$ , is encoded by the matrix  $\mathbf{G}^k$ . This matrix is critical for representing the time-varying heat input from each source into the system, allowing for a direct coupling between the source activity and the resulting temperature field. The matrix  $\mathbf{C}$  encodes the positions of fixed sensors within the domain, which are instrumental in monitoring the system's response to the dynamic heating conditions. Lastly, the

vector  $\mathbf{H}$  is a constant vector defined as  $\mathbf{H} = (\Delta_t \cdot 2h \cdot \theta_0) / (\rho C \cdot e)$ . It is determined by the system's discretization parameters, including the time step  $\Delta_t$ , and its physical properties such as  $\rho C$ ,  $h$ ,  $\theta_0$  and  $e$ , ensuring a precise representation of the thermal environment.

This numerical framework, incorporating the matrices  $\mathbf{L}$ ,  $\mathbf{B}^k$ ,  $\mathbf{G}^k$ , and the vector  $\mathbf{H}$ , alongside the fixed sensor matrix  $\mathbf{C}$ , allows to create a comprehensive numerical model that effectively captures both the static and dynamic aspects of heat transfer induced by moving heat sources. The finite difference approach (see for example Strikwerda, 2004 and LeVeque, 2007) provides a robust platform for the integration of these components, facilitating a precise simulation of the heat distribution across the plate.

The direct problem described by Equation (6) can be solved numerically when all input parameters of the model are determined using Matlab software (Figure 4). In Figure 4, the temperature variation on the plate is presented at a specific time of 3600s, demonstrating the absence of any failures in the three heat sources. This observation corresponds to their expected and normal behavior. Finally, Figure 5 depicts the observed temperature  $\mathbf{T}_{obs}^k$ , captured by four sensors. The sensor measurements are subject to a Gaussian noise level of  $\sigma = 1^\circ$ .

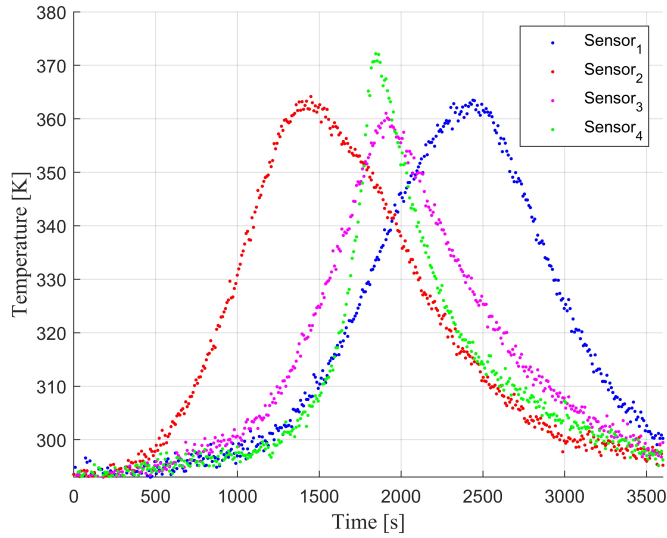
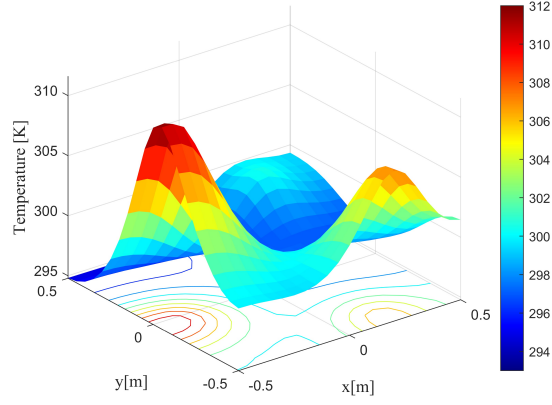
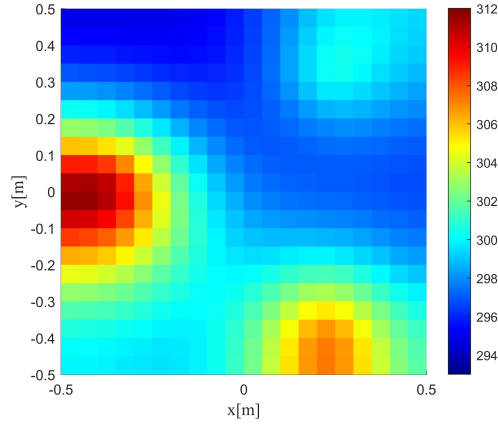


Figure 5.: Measurement data provided by the four sensors without failures.



(a) Results of the Direct Problem in 2D Geometry with 3D Visualization



(b) Results of the Direct Problem in 2D Geometry with 2D Visualization

Figure 4.: Solving the direct problem using finite difference method: Temperature distribution at  $t=3600s$  under normal operating conditions (no failures).

### 3.2. The Bayesian filter

With the assumption that both the evolution and observation models defined in system (6) are linear, the Kalman filter was used. In such models, it is assumed that the noises are Gaussian with known means and covariances, and that they are additive. The system (6) is then modified as follows:

$$\begin{cases} \mathbf{T}^{k+1} = \mathbf{L} \cdot \mathbf{T}^k + \mathbf{B}^k \cdot \mathbf{G}^k + \mathbf{H} + \mathbf{w}_k, \\ \mathbf{T}_{obs}^k = \mathbf{C} \cdot \mathbf{T}^k + \mathbf{v}_k, \end{cases} \quad (7)$$

where  $\mathbf{w}_k$ ,  $\mathbf{v}_k$  are the evolution and observation noises respectively with zero means and covariances matrices  $\mathbf{Q}$  and  $\mathbf{R}$  respectively. To estimate the input vector  $\mathbf{G}^k$ , a technique involves modifying the classical Kalman filter to incorporate the input vector into the state vector. By including the input vector, we can estimate the behavior of the heat flux  $\phi_i^k$  for each source ( $i = 1, \dots, 3$ ). This estimation of the heat flux behavior provides valuable insights and aids in identifying potential failures in the heat sources. The evolution and observation models may be respectively expressed as follows:

$$\begin{cases} \mathcal{T}^{k+1} = \mathcal{L}^k \cdot \mathcal{T}^k + \mathbf{H}' + \mathbf{w}'_k, \\ \mathbf{T}_{obs}^k = \mathbf{C}' \cdot \mathcal{T}^k + \mathbf{v}_k, \end{cases} \quad (8)$$

where:

$$\mathcal{T}^{k+1} = \begin{bmatrix} \mathbf{T}^{k+1} \\ \mathbf{G}^{k+1} \end{bmatrix}, \quad \mathcal{L}^k = \begin{bmatrix} \mathbf{L} & \mathbf{B}^k \\ \mathbf{0} & \mathbf{I} \end{bmatrix} \quad \text{and} \quad \mathbf{C}' = \begin{bmatrix} \mathbf{C} & \mathbf{0} \end{bmatrix}.$$

Figure 6 shows the integrated procedure using the Kalman filter. Finally, after reformulating the system (7) into (8) with the integration of the input vector  $\mathbf{G}$  into the state vector, we are ready to use the Kalman filter. The posteriori density is Gaussian and the Kalman filter gives the optimal solution to the state estimation problem.  $\mathcal{L}^k$  and  $\mathbf{C}'$  are given matrices for the corresponding state  $\mathcal{T}^k$  and observation  $\mathbf{T}_{obs}^k$ , also,  $\mathbf{H}'$  is a constant vector for the model of the state evolution  $\mathcal{T}^k$ , and  $\mathbf{I}$  is the matrix identity. In the following,  $\mathcal{T}$  is a Gaussian with calculable mean and covariance. We denote by  $\boldsymbol{\mu}$  and  $\boldsymbol{\Sigma}$  the means and covariance, respectively. Given that  $\mathbf{Q}'$  and  $\mathbf{R}$  are also Gaussian. Considering the noises,  $\mathbf{w}'$  with zero mean multivariate normal distribution  $\mathcal{N}$  and covariance matrix  $\mathbf{Q}'$ :  $\mathbf{w}' \sim \mathcal{N}(0, \mathbf{Q}')$ , and  $\mathbf{v}$  with a zero mean and covariance matrix  $\mathbf{R}$ :  $\mathbf{v} \sim \mathcal{N}(0, \mathbf{R})$ . The prediction and update steps of the Kalman filter, for each  $k = 1, \dots, t^*$ , where  $t^* = t_f / \Delta t_{obs}$ , are given by Algorithm 1.

The Kalman gain matrix is represented by  $\mathbf{K}_k$  in this algorithm,  $\mathbf{T}_{obs}^k$  is the observation vector at time  $k$ . In the application, temperatures are not measured at each time (they are only measured every 9 seconds), therefore if there is no measurement at time  $k$ , then  $\hat{\boldsymbol{\mu}}_{k|k} = \hat{\boldsymbol{\mu}}_{k|k-1}$ . To determine the different instants of failure and restart

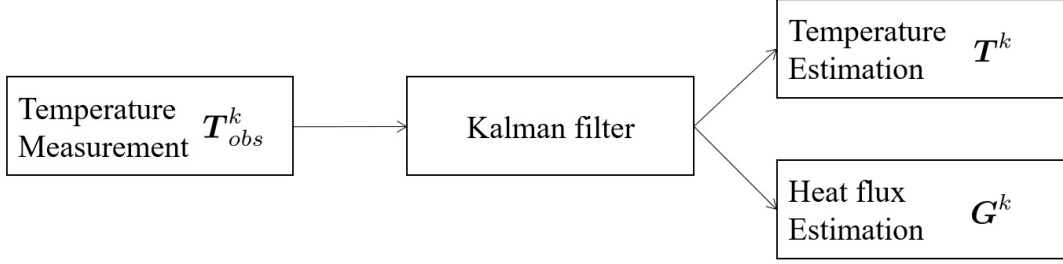


Figure 6.: Kalman filter schema.

---

**Algorithm 1** Kalman filter.

---

- i. Initialize:  $\hat{\boldsymbol{\mu}}_{0|0}$  and  $\boldsymbol{\Sigma}_{0|0}$ .
- ii. For  $k = 1, 2, \dots, t^*$ :

**Prediction:**

$$\hat{\boldsymbol{\mu}}_{k|k-1} = \mathcal{L}_k \hat{\boldsymbol{\mu}}_{k-1|k-1} + \mathbf{H}', \quad (9)$$

$$\hat{\boldsymbol{\Sigma}}_{k|k-1} = \mathcal{L}_k \hat{\boldsymbol{\Sigma}}_{k-1|k-1} \mathcal{L}_k^T + \mathbf{Q}. \quad (10)$$

**Update:**

$$\mathbf{K}_k = \hat{\boldsymbol{\Sigma}}_{k|k-1} \mathbf{C}'^T \left( \mathbf{C}' \hat{\boldsymbol{\Sigma}}_{k|k-1} \mathbf{C}'^T + \mathbf{R} \right)^{-1}, \quad (11)$$

$$\hat{\boldsymbol{\mu}}_{k|k} = \hat{\boldsymbol{\mu}}_{k|k-1} + \mathbf{K}_k \left( \mathbf{T}_{obs}^k - \mathbf{C}' \hat{\boldsymbol{\mu}}_{k|k-1} \right), \quad (12)$$

$$\hat{\boldsymbol{\Sigma}}_{k|k} = \left( \mathbf{I} - \mathbf{K}_k \mathbf{C}' \right) \hat{\boldsymbol{\Sigma}}_{k|k-1}. \quad (13)$$


---

of the sources, we will assume an offline analysis of this application. In this scenario, the Kalman smoother (Murphy, 2012) likewise known as Rauch-Tung-Striebel (RTS) smoother (Rauch et al., 1965) could provide a more accurate estimate of the state vector. For this algorithm, we assume that the Kalman filter has already been applied; the reverse steps are detailed in Algorithm 2.

### 3.3. Estimation methodology

To estimate the failure time  $t_{\text{fail}}$  and the restart time  $t_{\text{rest}}$ , an assumption was made that the failures of the sources are independent events, allowing them to be treated individually. Furthermore, the knowledge of the theoretical signal of each source without failure, denoted as  $\phi_i^k$  and graphically represented in Figure 2, was utilized. Given a set of candidate vectors  $\mathcal{Q}_{\text{cand}}$ , the problem is to find the optimal candidate vector

---

**Algorithm 2** Kalman Smoother.

---

- i. Initialize:  $\hat{\boldsymbol{\mu}}_{t^*|t^*}, \hat{\boldsymbol{\Sigma}}_{t^*|t^*}$ .
- ii. For  $k = t^* - 1, t^* - 2, \dots, 1$ :

$$\begin{aligned}\mathcal{P}_k &= \hat{\boldsymbol{\Sigma}}_{k|k} \mathbf{L}_k^T \hat{\boldsymbol{\Sigma}}_{k+1|k}^{-1} \\ \hat{\boldsymbol{\mu}}_{k|t^*} &= \hat{\boldsymbol{\mu}}_{k|k} + \mathcal{P}_k (\boldsymbol{\mu}_{k+1|t^*} - \hat{\boldsymbol{\mu}}_{k+1|k}) \\ \hat{\boldsymbol{\Sigma}}_{k|t^*} &= \hat{\boldsymbol{\Sigma}}_{k|k} + \mathcal{P}_k (\boldsymbol{\Sigma}_{k+1|t^*} - \hat{\boldsymbol{\Sigma}}_{k+1|k}) \mathcal{P}_k^T.\end{aligned}$$

---

$\varrho_{\text{opt}}$  that minimizes the squared error (SE) between  $\phi_i^k \times \varrho_{\text{cand}}^i$  and  $\hat{\phi}_i^k$ .

Mathematically, this can be expressed as follows:

$$\varrho_{\text{opt}}^i = \underset{\varrho_{\text{cand}}}{\text{Arg min}} \sum_k^{t^*} \left( \phi_i^k \times \varrho_{\text{cand}}^i - \hat{\phi}_i^k \right)^2, \quad (14)$$

where  $\varrho_{\text{cand}}^i$  represents the candidate vector which corresponds to source  $i$ ,  $\phi_i^k$  is the theoretical signal of each source without failure, and  $\hat{\phi}_i^k$  is the estimated flux of  $\phi_i^k$ .

Thus, for each source, the following algorithm can be used:

---

**Algorithm 3** Search strategy algorithm.

---

- i. Initialize and define the bounds of the candidate vector  $\varrho_{\text{cand}}^i$ .
  - ii. Compute the squared error (SE) between  $\phi_i(t) \times \varrho_{\text{cand}}^i$  and  $\hat{\phi}_i(t)$ .
  - iii. Solve problem (14) by performing an iterative search to find the value of  $\varrho_{\text{cand}}^i$  that minimizes the squared error, while respecting the constraints defined by the bounds.
  - iv. Return the optimal value of  $\varrho_{\text{opt}}^i$  that minimizes the squared error, along with the minimum value of the squared error.
- 

### 3.4. Illustration of the proposed methodology

For the purpose of demonstrating the proposed methodology, let us consider the scenario when the first mobile heat source  $q_1$  fails at  $t = 1500s$  within a one-hour monitoring period (3600s). The sources are the same as shown in Figure 2, we can apply the Kalman filter and then the Kalman smoother after we get the measurements data (Figure 7), and we obtain the signals shown in Figure 8 for  $\phi_1$ . Finally, with the  $\hat{\phi}_1$  estimated by a Kalman smoother, we may use the search technique described in the

previous subsection. Figure 9 depicts the multiple  $\phi_1$ : the theoretical heat flux, the real failure, the estimated by Kalman smoother, and the optimum computed candidate. The best selected candidate gives his failure instant at  $t_{\text{fail}}^1 = 1503\text{s}$ .

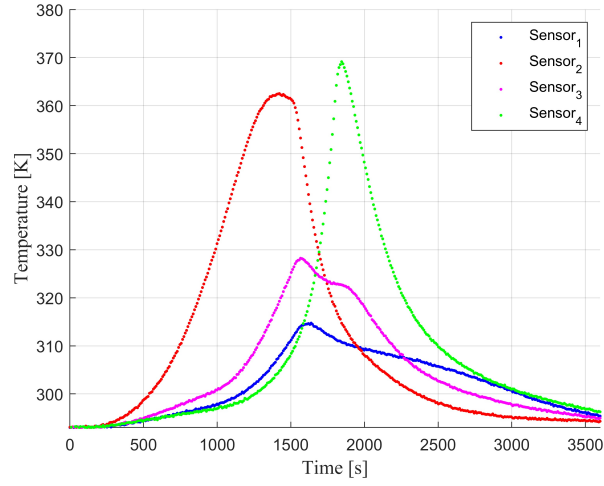


Figure 7.: Measurements data with  $\sigma = 0.1^\circ$ .

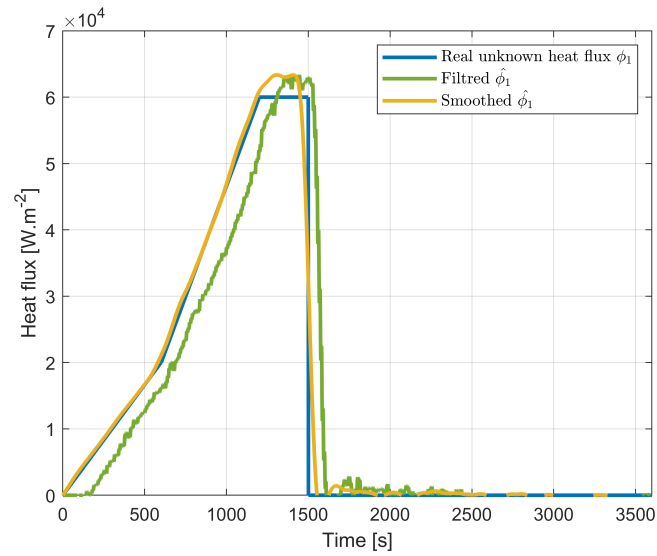


Figure 8.: Estimated heat flux  $\phi_1(t)$  by using Kalman filter and smoother.

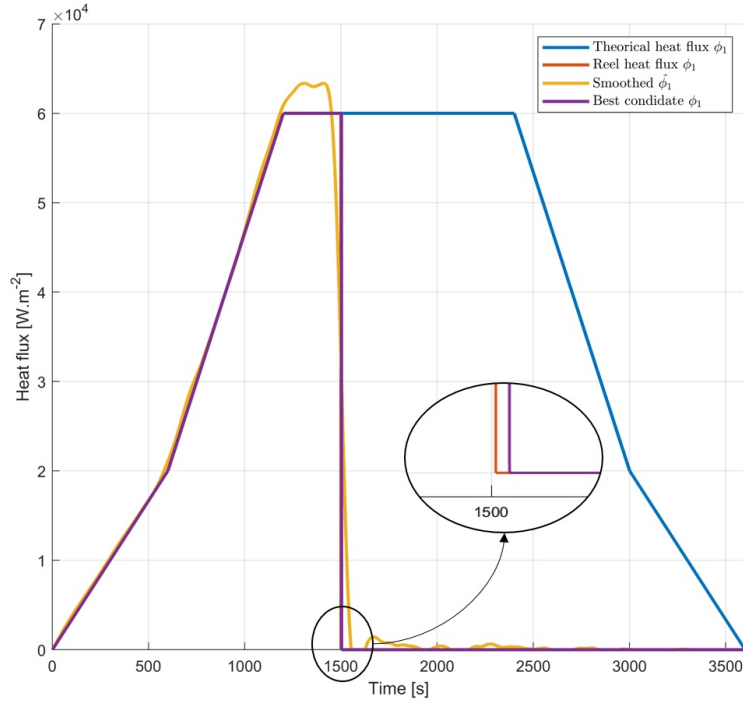


Figure 9.: The chosen candidate provides his failure instant at  $t_{\text{fail}}^1 = 1503\text{s}$ .

In the next section, a general study will be conducted, starting with the case of fixed sources, followed by mobile sources, to highlight the search approach based on the Kalman smoother (KS) technique for determining the failure times and switching instants for one or more mobile heat sources.

## 4. Numerical results

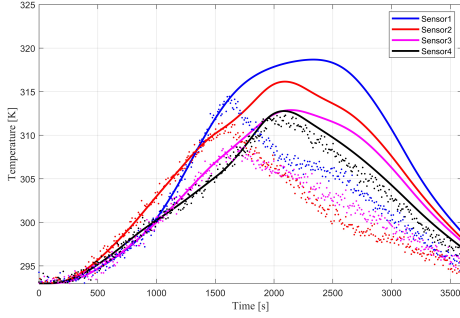
### 4.1. Fixed sources

Let's analyze the illustrative setting when the 3 sources are fixed. The mathematical model parameters are listed in Table 2. Matlab has been used to evaluate the data collected from a Comsol-Multiphysics simulation (preventing inverse crime). The four sensors' data uncertainty is represented by a Gaussian noise with a zero mean and different  $\sigma$  standard deviations, similarly to a real system. In order to adequately understand the impact of this parameter, the mean and standard deviation (in brackets) of 30 simulations for each configuration are presented. Let suppose that the first heat source has a failure time  $t_{\text{fail}}^1 = 1500\text{s}$ . The evolution of the temperatures at the four

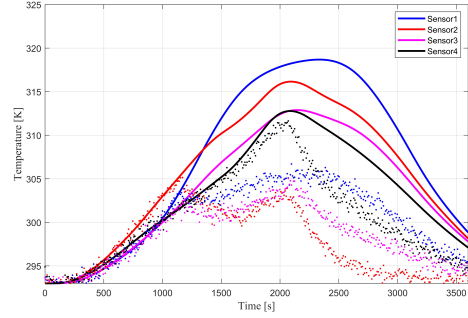
sensors  $C_1, C_2, C_3, C_4$  are shown in Figure 10a.

Table 2.: Mathematical model parameters.

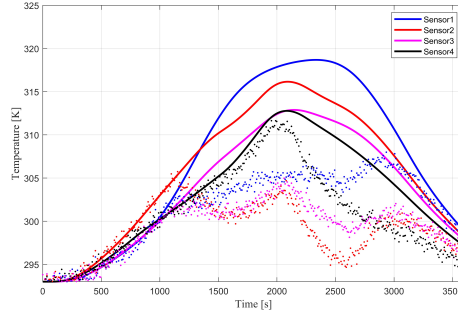
Symbol	Definition	Values
$\rho C$	Volumetric heat	$2.421 \cdot 10^6 \text{ J} \cdot \text{m}^{-3} \cdot \text{K}^{-1}$
$h$	Natural convection coefficient	$10 \text{ W} \cdot \text{m}^{-2} \text{K}^{-1}$
$\lambda$	Thermal conductivity	$178 \text{ W} \cdot \text{m}^{-1} \cdot \text{K}^{-1}$
$T_0$	Initial temperature	293 K
$t_f$	Final time	3600 s
$e$	Thickness	$2 \cdot 10^{-3} \text{ m}$
$\Delta t$	Time step	3 s
$\Delta t_{obs}$	Time step of the observations	9 s
$\Delta x, \Delta y$	Space step	0.05m



(a) Case when the heat source  $q_1$  fail.



(b) Case where source  $q_1$  and  $q_2$  fails.



(c) Case source  $q_1$  and  $q_2$  fails with restart of the first source  $q_1$ .

Figure 10.: Sensor Measurements: without any failure and noise, represented as continuous data, and with failure and noise, represented as discrete points.

Numerical results are obtained using Matlab software with a personal computer having the following characteristics: CPU: Intel<sup>®</sup> Core<sup>(TM)</sup> i5-10210U CPU 2.11 GHz, RAM: 8.00 Go, OS: Windows 10 (64). The results are given in Table 3 with different

noise levels. With this approach, it is clear that the search strategy gives a good result for estimating the failure times, when the noise levels of the sensors are less significant. However, the accuracy of the failure time detection is reduced considerably due to the increase in the measurement noise of the sensors.

Table 3.: Heat source  $q_1$  failure times with different noise levels.

	Failure $t_{\text{fail}}^1$
$\sigma = 0.1^\circ\text{C}$	1500s (1.03)
$\sigma = 0.5^\circ\text{C}$	1516.9s (3.09)
$\sigma = 1^\circ\text{C}$	1531.5s (6.19)

#### 4.1.1. Source separation

The objective in this new scenario is to identify the exact failure instants when two different sources experience failures. Specifically, we assume that the first source fails at  $t_{\text{fail}}^1 = 1000\text{s}$  and the second source fails at  $t_{\text{fail}}^2 = 2000\text{s}$ . For example, the measurements at the four sensors are given in Figure 10b with standard deviation  $\sigma = 0.5^\circ$ . By using the parameters listed in Table 2, we obtained the results presented in Table 4.

Table 4.: Heat sources  $q_1$  and  $q_2$  failure times.

	Failure $t_{\text{fail}}^1$	Failure $t_{\text{fail}}^2$
$\sigma = 0.1^\circ\text{C}$	1001(2.17)	2003(2.31)
$\sigma = 0.5^\circ\text{C}$	1003.2(5.06)	2008.9(4.41)
$\sigma = 1^\circ\text{C}$	975.8(9.21)	2041.7(7.68)

In Table 4, it is evident that approach have successfully identified the failure instants for two separate sources. When the measurement noises are less significant, the methods produce excellent outcomes. However, when the measurement noise of the sensors are increased, it becomes more difficult to identify the failure instants of the two sources.

#### 4.1.2. Identifying the failure and restart with source separation

The objective in this new scenario is to not only identify the failure instants for two distinct sources using the provided approach, but also identify when the sources restart (resume heating). In this particular configuration, we assume that the first source fails

at  $t_{\text{fail}}^1 = 1000\text{s}$  and then restarts at  $t_{\text{rest}}^1 = 2500\text{s}$ , while the second source fails at  $t_{\text{fail}}^2 = 2000\text{s}$ . The measurements recorded by the four sensors are depicted in Figure 10c, with a standard deviation of  $\sigma = 0.5^\circ$ . With the same parameters as before, we have obtained the results presented in Table 5.

Table 5.: Failure and restart times for  $q_1$  and failure times for  $q_2$ .

	Failure $t_{\text{fail}}^1$	Failure $t_{\text{fail}}^1$	Restart $t_{\text{rest}}^1$
$\sigma = 0.1^\circ\text{C}$	1001.4(1.4)	2005(1.4)	2504.5(1.14)
$\sigma = 0.5^\circ\text{C}$	999.5(3.92)	2014(5.15)	2513.8(4.09)
$\sigma = 1^\circ\text{C}$	976.7(8.41)	2041.2(6.44)	2539.4(5.68)

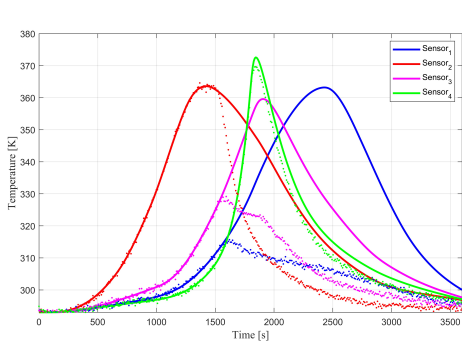
In the table above, the approach successfully identified the failure and restart times. We acquire a reasonable result when the measurement noise is less substantial; when it becomes more severe, the switching instants are marginally less precisely identified. In conclusion, the above table indicates the usefulness of the method for determining the failure and restart instants in the scenario of fixed heat source separation.

#### 4.2. Mobile sources

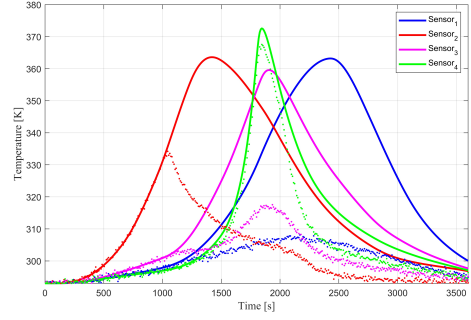
After studying the case of fixed sources and evaluating the performance of the methodology, we will now investigate the more complex case where the heat sources are mobile. Each heat source's exact trajectory is known (see Figure 1) with a constant velocity. The main challenge is to determine the failure and restart instants of this mobile heat sources, from the noisy measurements given by the fixed sensors. It is important to note that the failures exclusively impact the heating flux and do not affect the mobility of the sources. Let's start by supposing the first mobile heat source  $q_1$  has a failure time  $t_{\text{fail}}^1 = 1500\text{s}$ . The model input parameters are given in the Table 2, the evolution of the temperatures at the four fixed sensors  $C_i$ ,  $i = 1, \dots, 4$  are shown in Figure 11a. The results are given in Table 6 with different noise levels.

Table 6.: Heat source  $q_1$  failure times with different noise levels.

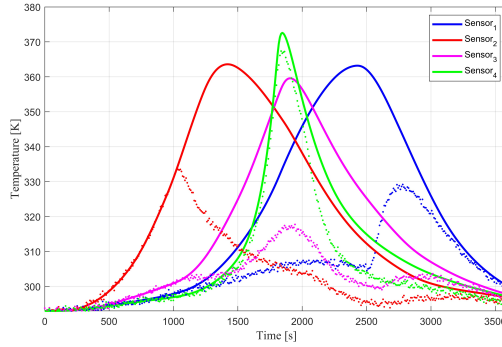
	Failure $t_{\text{fail}}^1$
$\sigma = 0.1^\circ\text{C}$	1503s (0.319)
$\sigma = 0.5^\circ\text{C}$	1505.9s (0.844)
$\sigma = 1^\circ\text{C}$	1505.2s (1.315)



(a) Case when the heat source  $q_1$  fail.



(b) Case when the heat sources  $q_1$  and  $q_2$  fails.



(c) Case when the source  $q_1$  and  $q_2$  fails with restart of the source  $q_1$ .

Figure 11.: Sensor Measurements: without any failure and noise, represented as continuous data, and with failure and noise, represented as discrete points.

When the sensor noise levels are less significant, it is obvious that the search strategy produces great results for calculating the failure times for this mobile heat source. However, when taking into account the number of sensors utilized for this specific application, the accuracy of the failure times identification is significantly improved compared to the case of fixed sources, due to reduced distance between the mobile heat source  $q_1$  and the fixed sensors.

#### 4.2.1. Source separation

After having successfully identified the failure instants for a single mobile heat source, The objective in this new scenario is to identify the failure instants for two distinct sources. In this configuration, we consider that first source  $q_1$  fails at  $t_{\text{fail}}^1 = 1000\text{s}$  and the second source  $q_2$  fails at  $t_{\text{fail}}^2 = 2000\text{s}$ . For example, the measurements at the four sensors are given in Figure 11b with standard deviation  $\sigma = 0.5^\circ$ . The results obtained

using the same parameters as before are summarized in Table 7.

Table 7.: Heat sources  $q_1$  and  $q_2$  failure times.

	Failure $t_{\text{fail}}^1$	Failure $t_{\text{fail}}^2$
$\sigma = 0.1^\circ\text{C}$	1002.7(0.606)	2004.1(0.48)
$\sigma = 0.5^\circ\text{C}$	999.4(1.52)	2007.7(1.30)
$\sigma = 1^\circ\text{C}$	999.8(3.98)	2009.8(2.8)

It is clear from the previous table that this method has successfully detected the failure instants for two distinct sources. When measurement noises are insignificant, the approach yields excellent results. However, when the measurement noise of the sensors is increased, the failure instants of the two sources have been identified with higher accuracy compared to fixed sources. As in the previous case, the effect of distance can be clearly seen in the obtained results.

#### 4.2.2. Identifying the failure and restart with source separation

After identifying the failure instants for two distinct sources using the proposed approaches, the challenge in this new scenario is to not only identify the failure instants, but also the restart (heating up again) of the sources. For this last configuration, we consider that first source  $q_1$  fails at  $t_{\text{fail}}^1 = 1000\text{s}$  then restarts at  $t_{\text{rest}}^1 = 2500\text{s}$  and the second source  $q_2$  fails at  $t_{\text{fail}}^2 = 2000\text{s}$ . For example, the measurements at the four sensors are given in Figure 11c with standard deviation  $\sigma = 0.5^\circ$ . Using the same parameters as before, we obtain the results presented in the Table 8

Table 8.: Failure and restart times for  $q_1$  and failure times for  $q_2$ .

	Failure $t_{\text{fail}}^1$	Failure $t_{\text{fail}}^2$	Restart $t_{\text{rest}}^1$
$\sigma = 0.1^\circ\text{C}$	998.6(0.498)	2009.6(0.5)	2509.2(0.406)
$\sigma = 0.5^\circ\text{C}$	989.4(1.79)	2027.4(1.1)	2512.7(0.98)
$\sigma = 1^\circ\text{C}$	984.1(3.19)	2042.9(3.82)	2514.6(1.65)

The approach has successfully identified the failure and restart times in the table shown above. When the measurement noise is less significant, we achieve a satisfactory result; when it becomes more significant, the switching instants are marginally better identified compared to the previous fixed case. In conclusion, the preceding table demonstrates the method's suitability for identifying failure and restart times in this problem characterized by parabolic partial differential equations.

## 5. Conclusion

This paper presents an approach for failure times identification in a heating system using a Bayesian filter. The focus of the research is on the challenging scenario of mobile heat sources with known trajectories. The proposed methodology involves two steps: applying a Bayesian filter to solve the IHCPs and employing a search strategy to estimate failure or restart times. By applying this approach, we can estimate failures and potential restart times for different mobile heat sources within a thermal system described by parabolic PDEs. The results demonstrate significant improvement compared to the case of fixed heat sources, highlighting the impact of the distance between the mobile heat source and fixed sensors. Several future research directions can be explored, including considering cases with varying velocities to examine their influence on result accuracy, incorporating mobile sensors for enhanced failure identification, and developing decision support methods for different scenarios within this framework, particularly for online detection and identification. Additionally, it is quite attractive to extend our research to include experimental implementation. This will involve constructing experimental setups that mirror our simulation scenarios, with a specific focus on replicating the trajectories of mobile heat sources and examining their interaction with sensor networks. This experimental validation is pivotal, as it will corroborate our theoretical results, bridging the gap between simulation-based predictions and real-world applications. It will provide valuable insights into the practical challenges and effectiveness of our Bayesian filter approach in dynamic thermal systems. Finally, we must not overlook the fact that confrontation with experimental set-ups often leads to the emergence of new problems and promising avenues of thought.

## 6. Acknowledgments

None.

## 7. Declaration of interest statement

The authors declare that they have no competing interests.

## 8. Data availability statement

The data that support the findings of this study are available from the corresponding author, upon reasonable request.

## References

- Alifanov, O. M. (1994). Iterative regularization of inverse problems. In *Inverse heat transfer problems* (pp. 227–328). Berlin, Heidelberg: Springer Berlin Heidelberg. Retrieved from [https://doi.org/10.1007/978-3-642-76436-3\\_9](https://doi.org/10.1007/978-3-642-76436-3_9)
- Ashby, M. F., & CEBON, D. (1993). Materials selection in mechanical design. *Le Journal de Physique IV*, 3(C7), C7–1.
- Autrique, L., Perez, L., & Scheer, E. (2009). On the use of periodic photothermal methods for materials diagnosis. *Sensors and Actuators B: Chemical*, 135(2), 478–487.
- Bidou, M. S., Perez, L., Verron, S., & Autrique, L. (2022b). Identification of failure times for a system governed by a non-linear parabolic partial differential equation. *IFAC-PapersOnLine*, 55(40), 37-42. Retrieved from <https://www.sciencedirect.com/science/article/pii/S2405896323000502> (1st IFAC Workshop on Control of Complex Systems COSY 2022)
- Bidou, M. S., Verron, S., Perez, L., & Autrique, L. (2022a). Kalman smoother for detection of heat sources defects. In *2022 international conference on control, automation and diagnosis (iccad)* (p. 1-6).
- Cai, J., Ferdowsi, H., & Sarangapani, J. (2016). Model-based fault detection, estimation, and prediction for a class of linear distributed parameter systems. *Automatica*, 66, 122-131. Retrieved from <https://www.sciencedirect.com/science/article/pii/S0005109815005609>
- Carslow, H., Jaeger, J. C., & Morral, J. (1986). Conduction of heat in solids. *Journal of Engineering Materials and Technology*, 108(4), 378–378.
- Cheng, M.-B., Radisavljevic, V., Chang, C.-C., Lin, C.-F., & Su, W.-C. (2009). A sampled-data singularly perturbed boundary control for a heat conduction system with noncollocated

- observation. *IEEE Transactions on Automatic Control*, 54(6), 1305–1310.
- Demetriou, M. A. (2002). A model-based fault detection and diagnosis scheme for distributed parameter systems: A learning systems approach. *ESAIM: Control, Optimisation and Calculus of Variations*, 7, 43–67.
- Duan, G.-R., & Patton, R. J. (2001). Robust fault detection using luenberger-type unknown input observers-a parametric approach. *International Journal of Systems Science*, 32(4), 533–540.
- El-Farra, N. H., & Ghantasala, S. (2007). Actuator fault isolation and reconfiguration in transport-reaction processes. *AIChE Journal*, 53(6), 1518–1537.
- Feng, Y., Wang, Y., Wang, J.-W., & Li, H.-X. (2022). Backstepping-based distributed abnormality localization for linear parabolic distributed parameter systems. *Automatica*, 135, 109930. Retrieved from <https://www.sciencedirect.com/science/article/pii/S0005109821004544>
- Ferdowsi, H., Cai, J., & Jagannathan, S. (2022). Actuator and sensor fault detection and failure prediction for systems with multi-dimensional nonlinear partial differential equations. *International Journal of Control, Automation and Systems*, 20(3), 789–802.
- Ferdowsi, H., Cai, J., & Jagannathan, S. (2023). Filter-based fault detection and isolation in distributed parameter systems modeled by parabolic partial differential equations. *IEEE Access*.
- Frank, P. M. (1994). On-line fault detection in uncertain nonlinear systems using diagnostic observers: a survey. *International journal of systems science*, 25(12), 2129–2154.
- Gaaloul, N., & Daouas, N. (2018). An extended approach of a kalman smoothing technique applied to a transient nonlinear two-dimensional inverse heat conduction problem. *International Journal of Thermal Sciences*, 134, 224–241. Retrieved from <https://www.sciencedirect.com/science/article/pii/S1290072918308238>
- Ghantasala, S., & El-Farra, N. H. (2009). Robust actuator fault isolation and management in constrained uncertain parabolic pde systems. *Automatica*, 45(10), 2368–2373.
- Ju, Y., Tian, X., Liu, H., & Ma, L. (2021). Fault detection of networked dynamical systems: A survey of trends and techniques. *International Journal of Systems Science*, 52(16), 3390–3409.
- Kaipio, J., & Somersalo, E. (2006). *Statistical and computational inverse problems*. Springer New York. Retrieved from <https://books.google.fr/books?id=h0i-Gi4rCZIC>
- Kaipio, J. P., & Fox, C. (2011). The bayesian framework for inverse problems in heat transfer.

- Heat Transfer Engineering*, 32(9), 718-753. Retrieved from <https://doi.org/10.1080/01457632.2011.525137>
- Kalman, R. E. (1960). A new approach to linear filtering and prediction problems.
- Krstic, M., & Smyshlyaev, A. (2008). *Boundary control of pdes: A course on backstepping designs*. SIAM.
- Lascoup, B., Perez, L., & Autrique, L. (2014). Defect localization based on modulated photothermal local approach. *Composites Part B: Engineering*, 65, 109–116.
- Lei, Y., Li, J., & Zhao, A. (2022). Spatiotemporal fault detection, estimation and control for nonlinear reaction-diffusion equations. *Applied Mathematics and Computation*, 418, 126859.
- LeVeque, R. J. (2007). *Finite difference methods for ordinary and partial differential equations: steady-state and time-dependent problems*. SIAM.
- Massard, H., Orlande, H., & Fudym, O. (2012). Estimation of position-dependent transient heat source with the kalman filter. *Inverse Problems in Science and Engineering*, 20(7), 1079–1099.
- Murphy, K. P. (2012). *Machine learning: a probabilistic perspective*. MIT press.
- Museux, N., Perez, L., Autrique, L., & Agay, D. (2012). Skin burns after laser exposure: Histological analysis and predictive simulation. *Burns*, 38(5), 658–667.
- Özisik, M. N., & Orlande, H. R. (2021). *Inverse heat transfer: fundamentals and applications*. CRC press.
- Özişik, M. N., Orlande, H. R., Colaco, M. J., & Cotta, R. M. (2017). *Finite difference methods in heat transfer*. CRC press.
- Patel, D. V., Ray, D., & Oberai, A. A. (2022). Solution of physics-based bayesian inverse problems with deep generative priors. *Computer Methods in Applied Mechanics and Engineering*, 400, 115428. Retrieved from <https://www.sciencedirect.com/science/article/pii/S004578252200473X>
- Pourdadashi Komachali, F., & Shafiee, M. (2020). Sensor fault diagnosis in fractional-order singular systems using unknown input observer. *International Journal of Systems Science*, 51(1), 116–132.
- Rauch, H. E., Tung, F., & Striebel, C. T. (1965). Maximum likelihood estimates of linear dynamic systems. *AIAA journal*, 3(8), 1445–1450.
- Strikwerda, J. C. (2004). *Finite difference schemes and partial differential equations*. SIAM.
- Vergnaud, A., Perez, L., & Autrique, L. (2016). Quasi-online parametric identification of

- moving heating devices in a 2d geometry. *International Journal of Thermal Sciences*, 102, 47–61.
- Wang, X., Zhang, D., & Zhang, L. (2020). Estimation of moving heat source for an instantaneous three-dimensional heat transfer system based on step-renewed kalman filter. *International Journal of Heat and Mass Transfer*, 163, 120435.
- Wen, S., Qi, H., Niu, Z.-T., Wei, L.-Y., & Ren, Y.-T. (2020). Efficient and robust prediction of internal temperature distribution and boundary heat flux in participating media by using the kalman smoothing technique. *International Journal of Heat and Mass Transfer*, 147, 118851.
- Wu, H.-N., & Li, H.-X. (2008).  $H_\infty$  fuzzy observer-based control for a class of nonlinear distributed parameter systems with control constraints. *IEEE Transactions on Fuzzy Systems*, 16(2), 502-516.
- Wu, H.-N., Wang, J.-W., & Li, H.-X. (2011). Exponential stabilization for a class of nonlinear parabolic pde systems via fuzzy control approach. *IEEE Transactions on Fuzzy Systems*, 20(2), 318–329.
- Yeonjong, Shin, , 9599, , Shin, Y., ... Karniadakis, G. E. (2020). On the convergence of physics informed neural networks for linear second-order elliptic and parabolic type pdes. *Communications in Computational Physics*, 28(5), 2042–2074. Retrieved from [http://global-sci.org/intro/article\\_detail/cicp/18404.html](http://global-sci.org/intro/article_detail/cicp/18404.html)
- Yin, M., Zheng, X., Humphrey, J. D., & Karniadakis, G. E. (2021). Non-invasive inference of thrombus material properties with physics-informed neural networks. *Computer Methods in Applied Mechanics and Engineering*, 375, 113603. Retrieved from <https://www.sciencedirect.com/science/article/pii/S004578252030788X>